MEMS for *In Situ* Testing—Handling, Actuation, Loading, and Displacement Measurements

M.A. Haque, H.D. Espinosa, and H.J. Lee

Abstract

Mechanical testing of micro- and nanoscale materials is challenging due to the intricate nature of specimen preparation and handling and the required load and displacement resolution. In addition, *in situ* testing requires the entire experimental setup to be drastically miniaturized, because conventional high-resolution microscopes or analytical tools usually have very small chambers. These challenges are increasingly being addressed using microelectromechanical systems (MEMS)-based sensors and actuators. Because of their very small size, MEMS-based experimental setups are the natural choice for materials characterization under virtually all forms of *in situ* electron, optical, and probe microscopy. The unique advantage of such *in situ* studies is the simultaneous acquisition of qualitative (up to near atomic visualization of microstructures and deformation mechanisms) and quantitative (load, displacement, flaw size) information of fundamental materials behavior. In this article, we provide a state-of-the-art overview of design and fabrication of MEMS-based devices for nanomechanical testing. We also provide a few case studies on thin films, nanowires, and nanotubes, as well as adhesion-friction testing with a focus on *in situ* microscopy. We conclude that MEMS devices offer superior choices in handling, actuation, and force and displacement resolutions. Particularly, their tight tolerances and small footprints are difficult to match by off-the-shelf techniques.

Introduction

Mechanical and electrical behavior of micro- and nanoscale materials are highly researched areas in materials science due to the ever-continuing miniaturization of microelectronics, data storage, micro/nanosensors and actuators, and energy conversion devices. It is well-known that microstructural and dimensional constraints, as well as the predominance of surfaces at the smaller scales, lead to significant differences in deformation and fracture mechanisms in these materials compared to the bulk.[1–4] Therefore, fundamental studies in synthesis-structure-properties are preferred over mere extrapolation of the scaling laws in materials behavior. However, the length scale of the specimens involved make characterization steps such as specimen preparation and handling, actuation, force, and displacement measurement with sufficient accuracy and tolerance extremely challenging.[5–8] For example, a typical nanowire tensile test may involve gripping and aligning of specimens that are a few tens of microns and nanometers in length and diameter respectively, requiring force and displacement resolution on the order of nanonewtons and nanometers, respectively.[9,10] While these are the basic requirements for quantitative testing, more rigorous requirements are needed for *in situ* testing, where the experiments are performed inside analytical chambers (such as electron and probe microscopes, which are typically very small, to accommodate conventional mechanical testing tools). For example, transmission electron microscopes (TEM) allow for visualization of dislocations, voids, grain, and phase boundaries with near atomic resolution;[11] however, TEMs typically allow only 3 mm × 3 mm × 0.5 mm work volume, which poses the challenge of miniaturizing and integrating the specimens with actuators and sensors.[12,13] Nevertheless, the unique advantage of seeing the microstructures and deformation mechanisms in real time while measuring the properties is worth the challenge, which is evident from the literature.[7,8,10,14] *In situ* testing is not only regarded as the ultimate characterization tool for the synthesis-structure-property relations in materials, but also for thermal, chemical,[15] magnetic, and electrical[16] phenomena.

Designing MEMS for Nanoscale Materials Testing

Earlier *in situ* studies involved conventional specimen preparation and actuation mechanisms[17–19] that lacked quantitative data on stress-strain and hence visualized a specimen's deformation as a function of strain only. The advent of microelectromechanical systems (MEMS) sensors and actuators opened up the possibility of truly quantitative testing in the TEM.[7,20,21] MEMS devices are fabricated using standard silicon-based microfabrication techniques, such as lithography, deposition, and etching, with the exception that MEMS structures are "released" from the substrate. This allows actuation of the devices using purely mechanical, thermal, or electrostatic phenomena. The advantages include small device dimensions; high force and displacement resolutions; tight tolerance on device-to-device performance offered by microfabrication techniques; the ability to integrate the specimen, the actuator and the force-displacement sensor as a lab-on-a-chip-type system for reliable handling; and a high degree of customization for a wide variety of mechanical testing.[13,22,23] Furthermore, as MEMS facilitate the transition from macro- to nanoscales, it is natural to combine the power of *in situ* microscopy with the versatile and precise measurement and actuation capabilities offered by MEMS. In this section, we discuss various MEMS designs opted for *in situ* electron and probe microscopy testing at the nanoscale.

Mechanical Sensing and Actuation

Figure 1 shows an example of purely mechanical actuation, where the specimen is suspended between a set of micromachined auto-alignment beams and a force sensing beam. The chip is pulled from the right end by an external piezoactuator, which imposes displacements on the specimen and the force sensor beam. The force (F) on the specimen is evaluated as $F = kd$, where k is the stiffness of the force sensor beam and d is the beam deflection, measured from micrographs. The stiffness of the force sensing beam is given by

$$k = \frac{24EI}{L^3}, \text{ where } I = \frac{1}{12} HW^3. \quad (1)$$

L, W, and H are the beam length, width, and height, respectively, E is the Young's modulus, and I relates the stiffness of the device to its beam dimensions. The force sensor beam thus can be designed to be extremely stiff or soft, depending upon the specimen material and dimensions. The two ends of the specimens have two sets of purely mechanical displacement sensors, which are rudimentary compared to capacitive or inductive schemes, but nonetheless are uninfluenced by the electron beam inside the microscope. The auto-alignment beams constrain the applied displacement only along the tensile axis of the specimen. Co-fabrication of the specimen with the device ensures that gripping of the specimen is due to its adhesion to the silicon substrate. This eliminates the necessity of an extra gripping mechanism for the specimen. In case of poor adhesion (such as gold with silicon), an adhesion-promoting intermediate layer can be used throughout the entire chip, except for the specimen gauge length. Also, nanoscale manipulation of the specimen on the device is possible for overly complicated co-fabrication processes.

One limitation of this design is that the mechanical displacement sensors on two ends of the specimen need to be in the field of view of imaging to obtain the quantitative measures of the applied force and displacement. This, in turn, limits the resolution with which the microstructure of the specimen can be imaged. Even though this limitation can be overcome in quasistatic experiments, as one can potentially zoom in on the specimen and maintain the same loading conditions, it requires adjusting the electron beam conditions, which can be inconvenient and can introduce artifacts. Therefore, automated sensing of loads and displacements is desirable. One such scheme employing electrothermal actuation and capacitive sensing is described next.

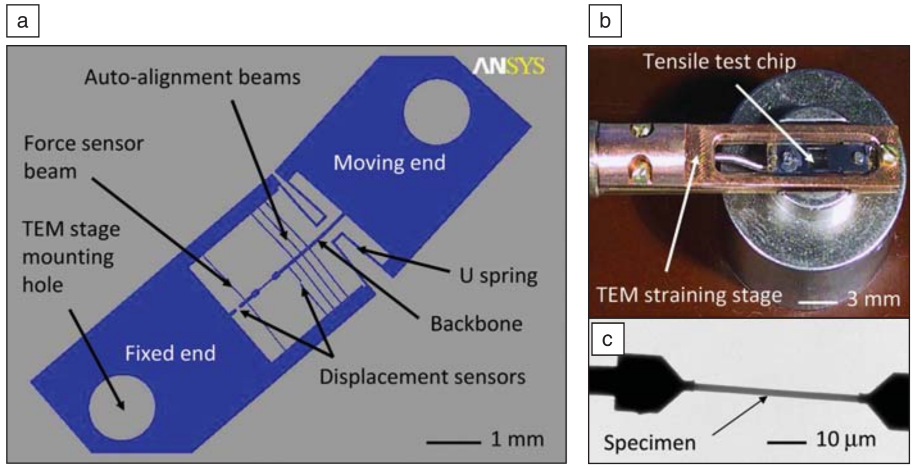

Figure 1. Microelectromechanical systems (MEMS)-based uniaxial tensile testing setup for *in situ* experiments inside the transmission electron microscope (TEM) with a purely mechanical actuation scheme. (a) Finite element representation of the MEMS device; the backbone transmits the externally applied displacement to the specimen. (b) Micromachined device placed on a custom TEM specimen holder. (c) Thin-film specimen imaged with the TEM. Reprinted with permission from Reference 50. ©2005, Materials Research Society.

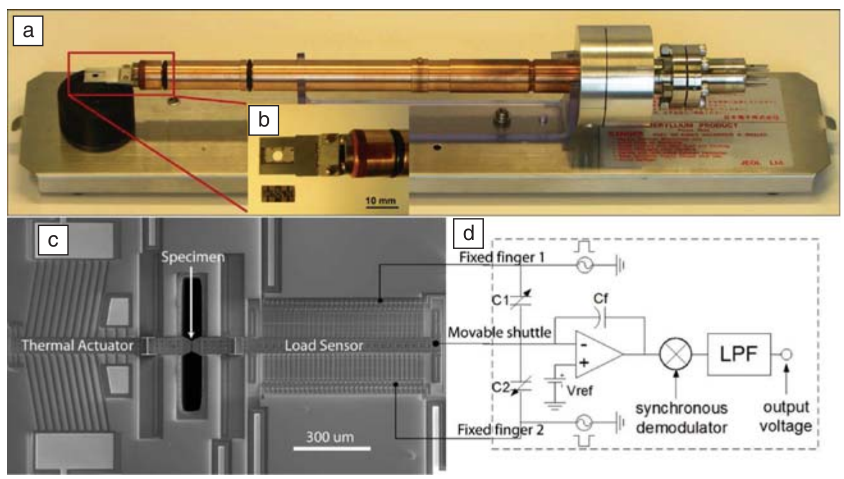

Figure 2. (a) Example of a transmission electron microscopy holder to interface a microelectromechanical system (MEMS)-based device with measurement electronics outside the electron microscopes. (b) A close-up view of the holder where the MEMS-based device is placed and the device. (c) Scanning electron microscopy micrograph of the MEMS-based mechanical testing device with thermal actuation and capacitive load sensing. (d) Schematic of the electronic circuitry employed to measure change in differential capacitance. C1 and C2, gap-dependent capacitors; LPF, low pass filter; Vref, reference voltage. (See Reference 13 for more details.)

Electrothermal Actuation and Capacitive Sensing

Figure 2 shows a setup developed for *in situ* TEM testing, where the displacements are applied using a thermal actuator, and the forces are measured electronically using differential capacitive sensors.[12,13] A special TEM holder (Figure 2a) is employed to interface the MEMS-based testing setup (shown in Figure 2c) with the outside electronics. The load in the specimen is transferred to the compliant load sensor shuttle, resulting in its motion, which eventually changes the gap between the parallel plates of the micromachined capacitors of the load sensor (shown in Figure 2c). The resulting change in differential capacitance is proportional to the deflection of the load sensor shuttle.[7,12,13] Hence, given the stiffness of the folded beams, the applied load is calculated, $F = kd$. Customized electronics have been developed to actuate the thermal actuator and to sense forces from the load sensor (as shown in Figure 2d). The ultimate resolution of the load depends on the base noise level of the electronics, which was experimentally determined to be on the order of a few nanonewtons.[7,24] Using the same physical principle and general idea, Zhang et al.[24,25] have recently developed a different geometrical arrangement utilizing bulk micromachining techniques.

The displacement applied to the specimen can be characterized by two different methods. The first and most common approach is by imaging and correlation of features in the sample. As the specimen is being directly imaged during the test, its strain can be inferred by cross-correlation of subsequent images, provided there are distinguishable features in the specimen. Such features can be the electron-beam- or ion-beam-induced deposited welds of carbon or platinum, which are used to fix the two ends of the specimen to the device. This is often the case both in scanning electron microscopy and TEM testing. In the case of TEM testing, this approach can be extended to a high resolution by measuring strain from selected-area diffraction patterns.[9] One such example of strain measurement is presented later in the context of ZnO nanowires. The second approach involves the usage of two differential capacitor sensors to allow the electronic measurement of sample elongation.[13]

The application of this state-of-the-art device is not limited to mechanical characterizations; recent modifications in the fabrication procedure allow for electrical isolation of the pads on which specimens are mounted. Additional conducting traces are laid to address these isolated pads and to probe the electrical response of the specimen. Therefore, combined with the existing features for mechanical testing, electromechanical coupling in a variety of conducting and semiconducting materials can be achieved through simultaneous mechanical and electrical characterization. In addition to these designs developed for uniaxial testing of one-dimensional and two-dimensional nanostructures, MEMS also have augmented conventional atomic force microscopy (AFM)-based nanoindentation to investigate thin-film specimens.

MEMS-Based In Situ *Probe Microscopy*

The versatility of MEMS as a tool for materials characterization is also evident from its capability for customization of existing techniques, such as AFM.[26,27] An example of MEMS-based enhancement of the conventional AFM testing is shown in Figure 3. Although AFM employs excellent force and displacement sensors, a conventional AFM cantilever is not appropriate for achieving the desired loading conditions in the nanoindentation tests.

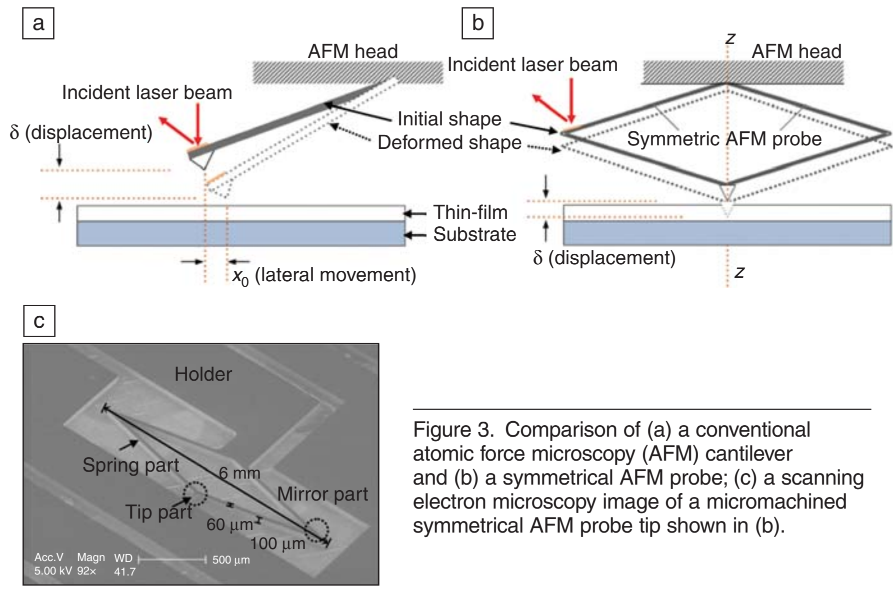

Figure 3. Comparison of (a) a conventional atomic force microscopy (AFM) cantilever and (b) a symmetrical AFM probe; (c) a scanning electron microscopy image of a micromachined symmetrical AFM probe tip shown in (b).

The conventional cantilever shown in Figure 3a has horizontal movement of the tip, as well as vertical movement when the tip is driven to move vertically. This horizontal movement is not critical in topographic measurement but can be a big obstacle in interpreting mechanical tests. For example, when indentation is performed using AFM, the tip should penetrate a sample perpendicular to the surface of the sample, and any horizontal movement should be compensated for or corrected to give accurate test results. This horizontal movement of the tip can be eliminated by an innovative design of the AFM probe with symmetrical geometry along the *z* axis, as shown in Figure 3b. Figure 3c shows an electron micrograph of the symmetrical probe fabricated using micromachining technology. In the next section, we present a few key results on mechanical-, electromechanical-, and nanoindentation-based testing using the techniques just described.

MEMS-Based Mechanical Testing

The capabilities of MEMS-based *in situ* TEM testing have been used to unravel many physical phenomena at the nanoscale, closing gaps between experimental findings and theoretical predictions. For example, the setup shown in Figure 2 was used to measure the mechanical properties of carbon nanotubes (CNTs).[8,28] These experiments, for the first time, revealed values close to the theoretical predictions, namely, an elastic modulus of ~1 TPa and fracture strength of ≈100 GPa. *In situ* high-resolution TEM (HRTEM) tests on individual multiwalled CNTs allowed for the characterization of chirality and the number of failing shells during tensile tests, thereby providing information about the load-bearing cross-section of the nanotubes (Figure 4a–c). In addition, it was found that the properties of the multiwalled CNTs can be tailored when exposed to various radiation doses with the TEM electron beam. The electron irradiation-induced cross-linkings between the nanotube shells increased their stiffness while preserving most of their strength. These experiments clearly demonstrate the power of combining HRTEM for near-atomic resolution and MEMS to obtain nanometer and nanonewton resolution in mechanical tests. The same experimental setup also has helped resolve the discrepancy regarding elasticity size effects in zinc oxide (ZnO) nanowires.[9,10] Experiments were conducted on nanowires as small as 20 nm in diameter, and they revealed that Young's modulus increases as the wire diameter decreases. These experimental findings were also complemented by atomistic simulations, where nanowires as large as 20 nm in diameter were modeled, bridging the gap between experimentally and computationally studied characteristic sizes. From the simulations, it was observed that atomic reconstruction on the surface results in reduced interatomic spacing, leading to increased elastic stiffness of surface atoms with respect to the bulk. This effect is dominant in smaller nanowires due to high surface-to-volume ratios and, therefore, the effective modulus of the nanowires increases as their diameter decreases. One of the key features of the tensile tests on ZnO nanowires included the atomic-level characterization of strain in the specimen from nanodiffraction

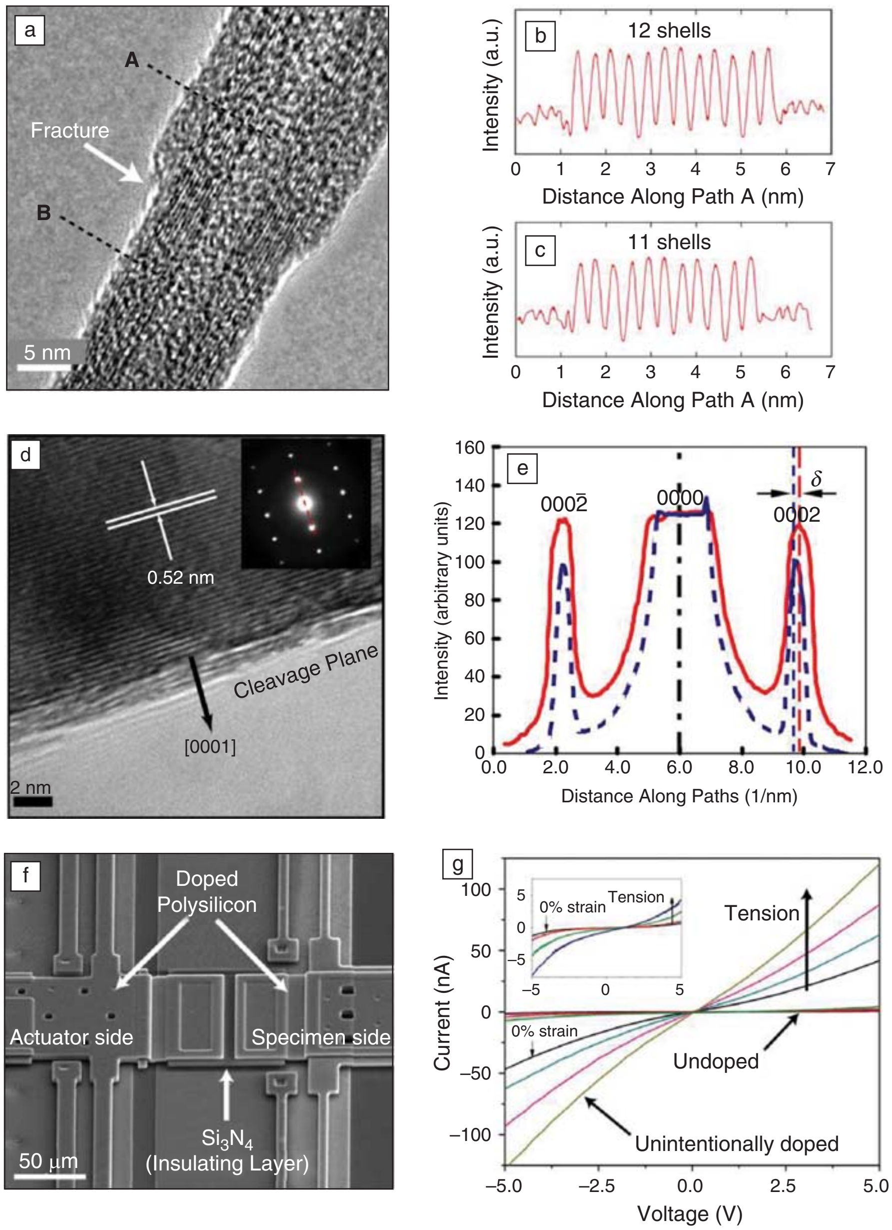

Figure 4. (a) Sword-in-sheath failure mode (outer few shells of a multiwalled nanotube fail, but inner walls remain intact and can be withdrawn like a sword) observed for multiwalled nanotubes; (b–c) intensity profiles along different cross-sections (indicated by lines A and B in section [a] of this figure) in the vicinity of the fracture zone confirming the number of shells that failed; (d) [0001] cleavage plane observed in ZnO nanowires under uniaxial tension (inset shows a diffraction pattern); (e) intensity profile along the red line in the inset for two diffraction patterns obtained at 0% and 2% strain. The shift in peak (δ) was then used to calculate the true atomic level strain; (f) scanning electron microscopy micrograph showing a modified device with a specimen isolated from actuating and sensing electronics; (g) change in current-voltage (*I–V*) response observed as a function of applied strain for gallium nitride nanowires. (See References 9,10, and 28 for more details.)

patterns obtained at different strain levels (Figure 4d–e).

Nanoscale thin films are a common form of specimen studied for fundamental understanding in the mechanics of deformation at the nanoscale.[19,29–31] Thin-film properties are sensitive to synthesis and processing conditions, hence different theories exist on their deformation mechanisms. One of these is based on smaller grain sizes, which cannot accommodate statistically significant dislocations.[32] There is evidence of dislocation starvation in the literature,[33–35] where pre-existing dislocations escape through surfaces, leaving behind a dislocation-free structure that requires higher stresses to nucleate and propagate new dislocations. However, it is also argued that dislocation-based plasticity can still manifest through their generation and motion through the grain boundaries.[36] Among other suggested mechanisms, grain-boundary sliding and diffusional creep are suggested to be dominant at the nanoscale because of their higher order of length-scale dependence.[37,38] Perhaps the most appealing application of MEMS in this research area is to provide direct and visual evidence of all these theories. For example, uniaxial tensile testing[20] in TEM supports the dislocation starvation concept and does not reveal appreciable grain-boundary sliding or diffusion, which explains why nanoscale metallic thin films may exhibit brittle-like mechanical properties. Another intriguing example is the plastic strain recovery in nanocrystalline gold films,[39] which is unambiguously shown to be driven by stress inhomogeneity in different grain sizes.

In principle, MEMS-based techniques can be applied to other forms of mechanical testing, including fracture, fatigue, and creep. An example of thin-film fracture study is given in Reference 40, where 100–125 nanometers-thick freestanding aluminum specimens with an average grain size of 50 nanometers were subjected to tensile loading *in situ* inside a TEM. A focused ion beam was used to create a notch with a radius and length of about 50 and 800 nanometers, respectively, before the loading. Figure 5 shows the stress-strain diagram as well as the TEM micrographs corresponding to several data points. Careful observation of the *in situ* TEM images shows only discrete dislocation activities in a few larger grains, which can be explained by comparing the minimum theoretically allowable distance between two dislocations (at least two of them are needed for a pileup) with the grain size.[41] Using linear elastic fracture mechanics, the fracture toughness is calculated to be about 0.7–1.1 MPa $m^{1/2}$, which is very low compared to the bulk value of about 20 MPa $m^{1/2}$ for pure aluminum. Such reduction in the stress intensity factor can be explained by the prevailing plane stress loading condition and the absence of any toughening mechanisms.[42] Significant changes in grain contrast, especially at the notch tip, were observed, which may be due to the rotation of the grains.

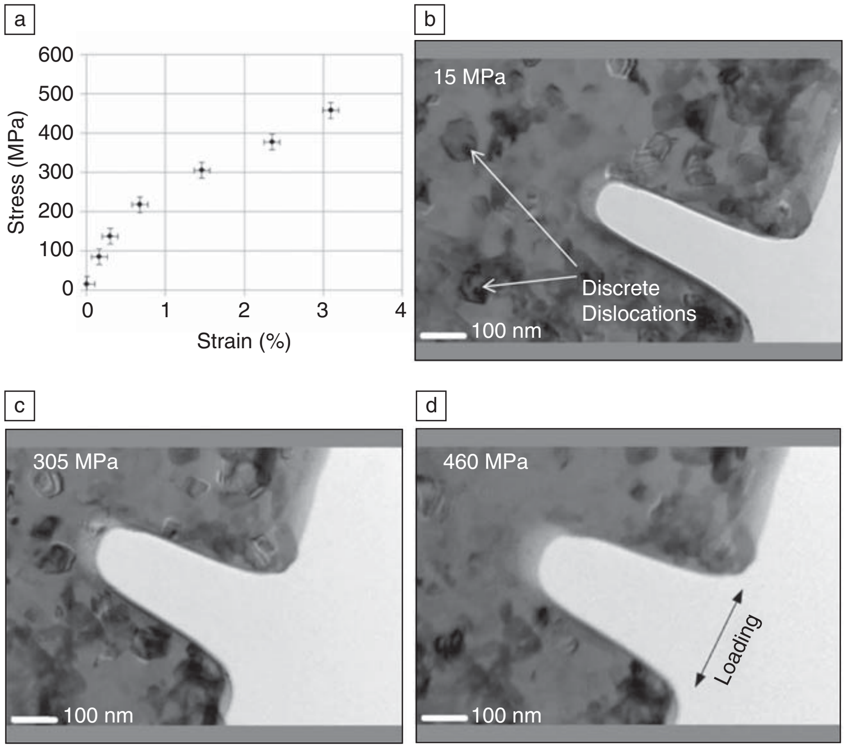

Figure 5. Experimental results on thin-film fracture experiments. (a) Stress-strain diagram for a notched aluminum specimen. *In situ* transmission electron microscopy images of the notched region at (b) 15 MPa, (c) 305 MPa, and (d) 460 MPa nominal stress. Reproduced with permission from the American Institute of Physics.

In situ TEM fracture experiments also reveal an interesting phenomenon called nanoscale flaw insensitivity, where the notched specimens do not fail at the notch, which has a stress concentration of about eight (local stress is about 4 GPa, which is very close to the theoretical failure stress). Such flaw insensitivity can be explained by scaling the classical fracture mechanics, for example, the Griffith criterion for crack growth, down to the nanoscale. Due to the length-scale effects on deformation and fracture mechanics, nanoscale specimens often exhibit theoretical strength. Therefore, for a specimen experiencing theoretical (or uniform rupture) strength, the classical notion of stress concentration ceases to bear the usual physical interpretation.[43]

MEMS-Based Electromechanical Testing

Due to the versatility provided by microfabrication and MEMS, new devices can be conceived to probe the coupling among various physical domains. For example, electromechanical coupling can be very strong in nanostructures[44,45] and requires simultaneous electrical and mechanical probing of the specimen. The two-terminal electrical addressing of a nanostructure on the device shown in Figure 2c has been achieved by introducing an insulating nitride layer between the thermal actuator and the specimen shuttle on one side, and the load sensor and specimen shuttle on the other side (Figure 4f).

With this device, coupled characterization of mechanical and electrical properties of a nanostructure is possible. For example, strain can be imposed incrementally to a nanowire, and the change in resistance can be measured in each step of increasing strain. With proper metrology, the piezoresistivity constant of the specimen can be extracted. This requires extensive characterization of the contact resistances between the nanostructure and the testing device and the properties of the sample-weld (electron beam–induced platinum deposition) interface. An example of the measured change of resistance for a GaN nanowire with applied tension is shown in Figure 4g for an undoped and unintentionally doped GaN nanowire. Both nanowires show piezoresistive behavior, and, as expected, the overall resistance is ~10 times higher for the undoped nanowire. The same setup was employed in the piezoelectric characterization of semiconducting nanowires.

MEMS-Based AFM Testing

Using the micromachined symmetrical AFM probe (described in the MEMS-Based In Situ Probe Microscopy section of this article), it is possible to perform various mechanical tests. Representative setups for several AFM-based test configurations are shown in Figure 6. In order to perform adhesion, strip-bending,[46] or indentation[46,47] tests using AFM with a symmetrical probe, a tip needs to be attached to the end of the probe during micromachining. The tip can be fabricated monolithically or attached to the probe afterward, depending on the nature of the test. The tip consists of a flat punch or a sphere for the adhesion test, a wedge for the strip-bending test, and a Berkovich tip or cube corner for indentation. In the actual tests, it is important to measure the deformation of the specimen accurately, because the AFM probe is very compliant, and the deformation of the probe is coupled to the load applied to the specimen. The deformation of the probe is usually compensated for after the strip-bending and indentation tests. The stiffness of the probe should be carefully chosen depending on the test application. The unique advantage of such probes with two-stage stiffness is that they can provide both topography and mechanical property measurement. This is because typically lower stiffness (on the order of 1 N/m) is desirable for measurement of surface topography, whereas orders-of-magnitude higher stiffness is required for mechanical tests.

Conclusions

The most stringent requirement for *in situ* testing of small-scale materials inside electron and probe microscopes is the overall experimental setup, which must be miniaturized drastically to be accommodated by these analytical tools. This has challenged researchers for decades, especially for *in situ* TEM testing. These issues can be efficiently addressed by MEMS sensor and actuators with small size, force, and displacement ranges, high-force and displacement resolution, and, most importantly, tight manufacturing and hence performance tolerances. In addition, microfabrication techniques can be used to prepare micro- and nanoscale specimens and integrate them with sensors and actuators. While MEMS-based setups are currently being applied to primarily mechanical testing, their versatility and customizability make them promising for studying coupling among other physical domains. Along with the miniaturization of testing setups employing MEMS, developments in electron microscopy (e.g.,

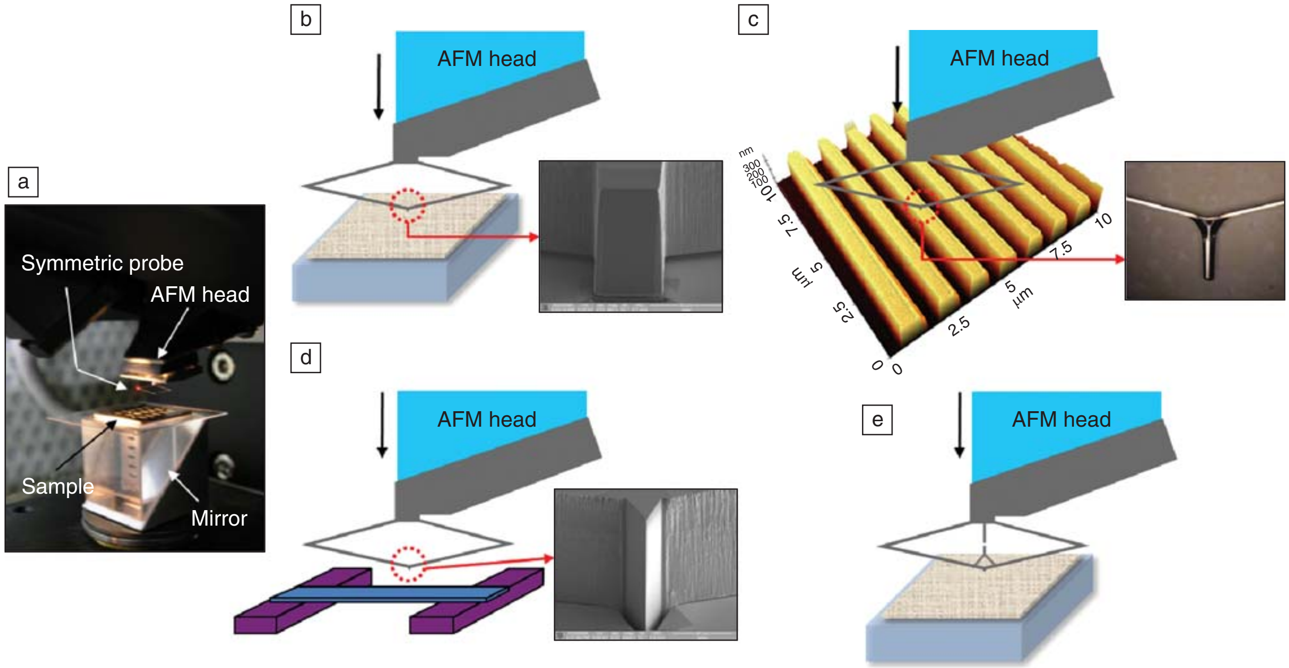

Figure 6. Typical experimental setup and test results using the symmetrical atomic force microscopy (AFM) probe. (a) An enlarged view of the AFM head; (b) the adhesion test; (c) indentation; (d) the strip-bending test; and (e) a mechanical test using a probe with two-stage stiffness.

improvements in the temporal resolution through better image acquisition)[48,49] can lead to the capturing of local events along with the quantitative measure of applied loads and displacements.

Acknowledgments

M.A. Haque gratefully acknowledges the support from the Center for Nanoscale Mechatronics & Manufacturing of the Korea Institute of Machinery & Materials and the National Science Foundation, USA (ECS #0545683). H.D. Espinosa acknowledges the support of the National Science Foundation through awards No. CMMI -0555734, DMR-0907196, and EEC – 0647560. The support from ONR through Award No. N00014-08-1-0108 and ARO through awards No. W911NF-08-1-0541 and W911NF-08-1-0061 are also greatly appreciated. H.D.E. would like to thank Dr. Ignacio Perez from ONR for his encouragement and support concerning the development of experimental methods to investigate electromechanical properties of CNTs and NWs. He also thanks I. Petrov and E. Olson for their contribution toward the manufacturing of the *in situ* TEM holder used in the work reported here. H.D.E. thanks N. Sanford and K. Bertness, from the National Institute of Standards and Technology, for providing GaN nanowires. H.J. Lee acknowledges the support (08-K1401-00610) from the Center for Nanoscale Mechatronics & Manufacturing, which is supported by the Ministry of Education, Science, and Technology in Korea.

References

1. E. Arzt, *Acta Mater*. **46**, 5611 (1998).
2. H. Van Swygenhoven, J.R. Weertman, *Mater. Today* **9**, 24 (2006).
3. I. Ovid'ko, *J. Mater. Sci*. **42**, 1694 (2007).
4. R. Agrawal, H.D. Espinosa, *J. Eng. Mater. Technol*. **131** 041208 (2009).
5. M.A. Haque, M.T.A. Saif, in *Handbook on Experimental Mechanics,* W.N. Sharpe, Ed. (Society of Experimental Mechanics, CT, 2008).
6. D.S. Gianola, C. Eberl, *JOM* **61**, 24 (2009).
7. Y. Zhu, H.D. Espinosa, *Proc. Nat. Acad. Sci. U.S.A*. **102**, 14503 (2005).
8. B. Peng, M. Locascio, P. Zapol, S. Li, S. L. Mielke, G.C. Schatz, H.D. Espinosa et al., *Nat. Nanotechnol*. **1**, 626 (2008).
9. R. Agrawal, B. Peng, E.E. Gdoutos, H.D. Espinosa, *Nano Lett*. **8**, 3668 (2008).
10. R. Agrawal, B. Peng, H.D. Espinosa, *Nano Lett*. **9**, 4177 (2009).
11. D.E. Newbury, D.B. Williams, *Acta Mater*. **48**, 323 (2000).
12. Y. Zhu, N. Moldovan, H.D. Espinosa, *Appl. Phys. Lett*. **86**, 013506 (2005).
13. H.D. Espinosa, Y. Zhu, N. Moldovan, *J. Microelectromech. Syst*. **16**, 1219 (2007).
14. I.M. Robertson, P.J. Ferreira, G. Dehm, R. Hull, E.A. Stach, *MRS Bull*. **33**, 122 (2008).
15. F. Banhart, Ed., *In-Situ Electron Microscopy at High Resolution* (World Scientific, NJ, 2008).
16. J. Cummings, E. Olsson, A.K. Petford-Long, Y. Zhu, *MRS Bull*. **33**, 101 (2008).
17. A. Couret, J. Crestou, S. Farenc, G. Molénat, N. Clément, A. Coujou, D. Caillard, *Microsc. Microanal. Microstruct*. **4**, 153 (1993).
18. U. Messerschmidt, *J. Phys*. **3** (7) Part 3, 2123 (1993).
19. G. Dehm, M. Legros, B. Heiland, *J. Mater. Sci*. **41**, 4484 (2006).
20. M.A. Haque, M.T.A. Saif, *Proc. Nat. Acad. Sci*. **101**, 6335 (2004).
21. M. Haque, M. Saif, *Exp. Mech*. **43**, 248 (2003).
22. B.G. Demczyk, Y.M. Wang, J. Cumings, M. Hetman, W. Han, A. Zettl, R.O. Ritchie, *Mater. Sci. Eng. A* **334**, 173 (2002).
23. J.H. Han, M.T.A. Saif, *Rev. Sci. Instrum*. **77**, 045102 (2006).
24. M. Zhang, E.A. Olson, R.D. Twesten, J.G. Wen, L.H. Allen, I.M. Robertson, I. Petrov, *J. Mater. Res*. **20**, 1802 (2005).
25. D. Zhang, W. Drissen, J.-M. Breguet, R. Clavel, J. Michler, *J. Micromech. Microeng*. **19**, 075003 (2009).
26. U. Lang, J. Dual, in *Applied Scanning Probe Methods XIII* (Springer, NY, 2009), pp. 165–182.
27. Y. Zhu, C. Ke, H.D. Espinosa, *Exp. Mech*. **47**, 7 (2007).
28. M. Locascio, B. Peng, P. Zapol, Y. Zhu, S. Li, T. Belytschko, H.D. Espinosa, *Exp. Mech*. **49**, 169 (2009).
29. R.C. Hugo, H. Kung, J.R. Weertman, R. Mitra, J.A. Knapp, D.M. Follstaedt, *Acta Mater*. **51**, 1937 (2003).
30. M. Legros, D.S. Gianola, K.J. Hemker, *Acta Mater*. **56**, 3380 (2008).
31. S.H. Oh, M. Legros, D. Kiener, P. Gruber, G. Dehm, *Acta Mater*. **55**, 5558 (2007).
32. D. Sen, M.J. Buehler, *Phys. Rev. B: Condens. Matter* **77**, 195439 (2008).

33. D. Wolf, V. Yamakov, S.R. Phillpot, A. Mukherjee, H. Gleiter, *Acta Mater*. **53**, 1 (2005).
34. H.D. Espinosa, S. Berbenni, M. Panico, K.W. Schwarz, *Proc. Nat. Acad. Sci*. **102**, 16933 (2005).
35. H. Tang, K.W. Schwarz, H.D. Espinosa, *Phys. Rev. Lett*. **100**, 185503 (2008).
36. B. Baretzky, M.D. Baró, G.P. Grabovetskaya, J. Gubicza, M.B. Ivanov, Y.R. Kolobov, *Rev. Adv. Mater. Sci*. **9**, 45 (2005).
37. Z.W. Shan, E.A. Stach, J.M.K. Wiezorek, J.A. Knapp, D.M. Follstaedt, S.X. Mao, *Science* **305**, 654 (2004).
38. A. Lin, M. Meyers, K. Vecchio, *Mater. Sci. Eng. C* **26**, 1380 (2006).
39. J. Rajagopalan, J.H. Han, M.T.A. Saif, *Science* **315**, 1831 (2007).
40. S. Kumar, M.A. Haque, H. Gao, *Appl. Phys. Lett*. **94**, 253104 (2009).
41. N. Wang, Z. Wang, K.T. Aust, U. Erb, *Acta Metall. Mater*. **43**, 519 (1995).
42. H. Hosokawa, A.V. Desai, M.A. Haque, *Thin Solid Films* **516**, 6444 (2008).
43. H. Gao, B. Ji, I.L. Jager, E. Arzt, P. Fratzl, *Proc. Nat. Acad. Sci. U.S.A.* **100**, 5597 (2003).
44. R. He, P. Yang, *Nat. Nano* **1**, 42 (2006).
45. T.W. Tombler, C. Zhou, L. Alexseyev, J. Kong, H. Dai, L. Liu, C.S. Jayanthi, M. Tang, S.-Y. Wu, *Nature* **405**, 769 (2000).
46. C.W. Baek, J.M. Kim, Y.K. Kim, J.H. Kim, H.J. Lee, S.W. Han, *Sens. Mater*. **17**, 277 (2005).
47. M.R. Van Landingham, *Microsc. Today* **97**, 12 (1997).
48. M.R. Armstrong, K. Boyden, N.D. Browning, G.H. Campbell, J.D. Colvin, W.J. DeHope, A.M. Frank, et al., *Ultramicroscopy* **107**, 356 (2007).
49. J.S. Kim, T. LaGrange, B.W. Reed, M.L. Taheri, M.R. Armstrong, W.E. King, N.D. Browning, G.H. Campbell, *Science* **321**, 1472 (2008).
50. M.A. Haque, M.T.A. Saif, *J. Mater. Res*. **20** (7), 1770 (2005).